

Compton electron scattering in the 0.1 to 5.0 GeV energy range

A. T. Goshaw, T. Glanzman, L. R. Fortney, W. J. Robertson, and W. D. Walker

Physics Department, Duke University, Durham, North Carolina 27706

(Received 22 February 1978)

We have measured the Compton electron spectrum coming from photons produced from the decays of π^0 mesons. The production rate agrees well with that predicted from the Klein-Nishina formula. The agreement, expressed as a ratio R between the predicted and the measured numbers of Compton electrons, is as follows: For Compton-electron energies between 0.1 and 5.0 GeV, $R = 1.03 \pm 0.07$; for energies between 0.8 and 5.0 GeV, $R = 0.95 \pm 0.14$.

I. INTRODUCTION

The scattering of photons by free electrons is one of the simplest and most basic quantum-electrodynamic processes that is experimentally accessible. Many theoretical calculations of the characteristics of this interaction have been made after the first semi-quantum-mechanical treatment was presented by A. H. Compton in 1922.¹ However, relatively few experimental measurements have been made at high energies. We present here results that include the first Compton-scattering measurements that have been made using photons over 1 GeV. In this introduction we first summarize the theoretically predicted characteristics of Compton scattering at high energies. We then review the experimental measurements that have been made using photons over 0.1 GeV. With this perspective established, we present our experimental procedure (Sec. II), the data obtained (Sec. III), and a comparison to theory (Secs. IV and V).

A. A summary of theoretical calculations

The correct QED treatment of the lowest-order scattering diagram [see Fig. 1(a)] was published by Klein and Nishina in 1929² and by Tamm in 1930.³ The general characteristics of Compton electron scattering, as predicted by the Klein-Nishina formula, are shown in Fig. 2 [see Fig. 1(b) for the laboratory scattering variables used throughout this paper]. The total cross section for photons in the energy range from 0.1 to 10 GeV is shown and also a typical differential cross section evaluated for 1-GeV photons. These illustrate two well-known features of Compton electron scattering at high energies: (i) the total cross section decreases approximately as $1/E$, and (ii) $d\sigma/d\Omega_e$ for the scattered electron is sharply peaked at small angles relative to the incident photon.

Two types of corrections to the basic Klein-Nishina formula must be considered when studying

Compton scattering at high energies (above 0.1 GeV). Figure 3(a) shows a typical radiative correction to single Compton scattering and Fig. 3(b) shows a diagram representing double Compton scattering in which there are two real photons in the final state. Double Compton scattering affects the measurement of single Compton scattering since a second very soft photon will not be detectable by the experimental apparatus.

The interference between the basic first-order amplitude and the radiative amplitude causes a suppression of the single-Compton-scattering total cross section below that predicted by the Klein-Nishina formula. This interference amplitude was first calculated by Brown and Feynman⁴ and the total cross section has been subsequently evaluated in a more convenient form by Anders⁵ and Mork.⁶ Using a result obtained by Mork, the effect of the radiative amplitude can be calculated easily and is shown in Fig. 4 (dashed curve) as a percentage

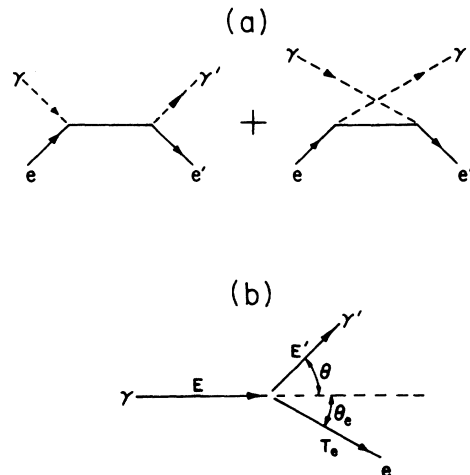


FIG. 1. (a) The lowest-order Feynman diagrams for Compton scattering. A QED calculation using these diagrams results in the Klein-Nishina formula. (b) Definition of the laboratory scattering variables used throughout this paper.

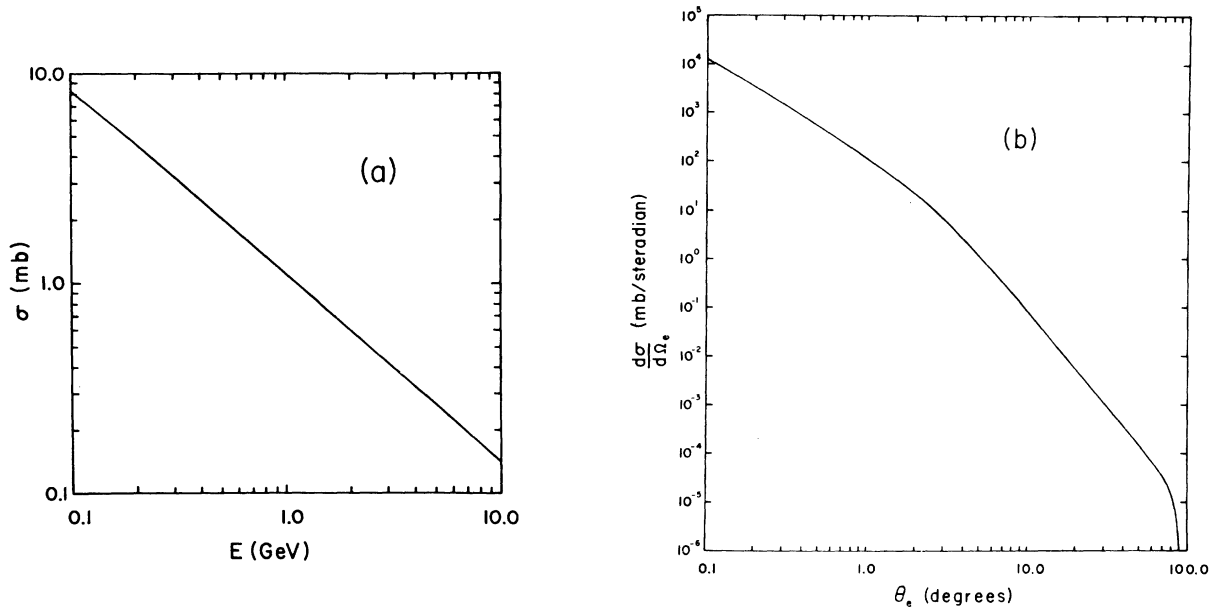


FIG. 2. Cross sections calculated using the Klein-Nishina formula; (a) the total cross section as a function of photon laboratory energy and (b) the laboratory differential cross section in terms of the scattered electron angle.

correction to the Klein-Nishina total cross section.⁷

The theory of double Compton scattering was first studied in detail by Mandl and Skyrme.⁸ Quantitative predictions require rather complicated numerical integrations and these have been considered by Anders,⁵ Ram and Wang,⁹ and Mork.⁶ We have used results obtained in Mork's paper to calculate the total double-scattering cross section in the photon-energy range from 0.1 to 1.0 GeV.¹⁰ This is shown in Fig. 4 (dotted curve) as a percentage correction to the Klein-Nishina total cross section. Mork did not extend his numerical integration results above 1 GeV, but calculations done by Ram and Wang suggest that the double-scattering total cross section increases by only about $\frac{1}{3}$ between 1 and 10 GeV.

The sum of the single and double Compton cross sections is given by the solid curve in Fig 4.¹¹ This is the total cross section for $\gamma e^- \rightarrow e^- +$ (one or two γ 's) and, because of the partial cancellation between the radiative correction and the double Compton effect, does not differ much from the Klein-Nishina total cross section for $\gamma e^- \rightarrow \gamma e^-$. We emphasize this point because it is sometimes not clearly stated in the theoretical literature.

B. A review of experimental measurements

Four measurements have been made using photon beams with energies over 0.1 GeV. They test different aspects of Compton scattering and find agreement with the Klein-Nishina formula to an

accuracy of from 10 to 15%.

Coengen¹² used a 0.25-GeV photon beam and measured the coincidence between the Compton-scattered photon and electron. His data for $d\sigma/d\theta_\gamma$ agree with the Klein-Nishina differential cross section to 10% for $4^\circ < \theta_\gamma < 25^\circ$. An experiment done by Kurnosova *et al.*,¹³ also used 0.25-GeV photons but measured only the scattered electron. They find that the cross section for electrons scattered with energies between 0.23 and 0.25 GeV agrees with the Klein-Nishina prediction to about 15%. Anderson *et al.*¹⁴ measured the total single-

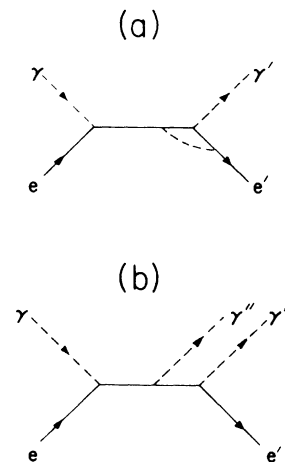


FIG. 3. (a) A typical radiative correction to single Compton scattering. (b) A Feynman diagram representing double Compton scattering.

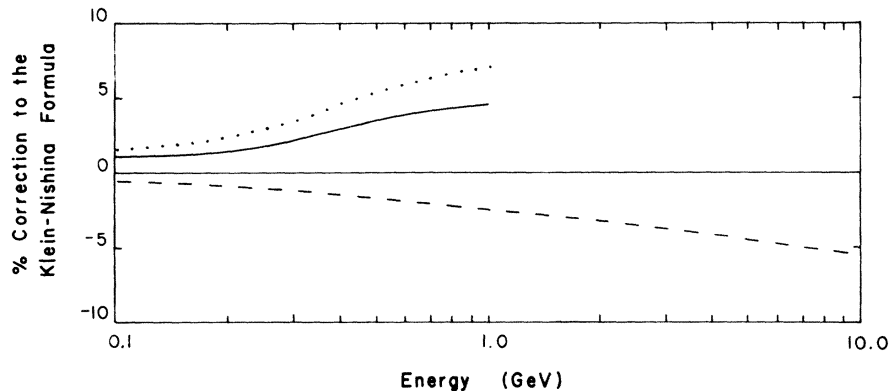


FIG. 4. The dashed curve shows the percentage correction to the Klein-Nishina formula caused by radiative corrections of the type shown in Fig. 3(a). The dotted curve shows the double-scattering cross section expressed as a percentage of the Klein-Nishina formula. The total percentage correction to the Klein-Nishina formula due to both effects is given by the solid curve.

plus-double Compton-scattering cross section using 0.32-GeV photons and found agreement with theory to about 15% (a photon total-absorption technique was used). Finally, Gittelmann *et al.*¹⁵ measured the cross section for the Compton scattering of a bremsstrahlung photon beam covering the energy range 0.2 to 0.95 GeV. They measured essentially the total Compton cross section since the experiment detected all electrons scattered at small forward angles. Their data agree with predictions of the Klein-Nishina formula to about 10%.

II. EXPERIMENTAL PROCEDURE

A. Photon source and flux measurement

The Compton electrons studied in this experiment were produced by photons coming from the hadronic interaction of 10.5-GeV/c π^+ mesons with nucleons. At least 90% of these γ 's come from the decay of π^0 mesons. The γ -production point and the Compton electron were both observed in the SLAC 82-in. bubble chamber filled with a hydrogen-neon mixture (32.2 molar percent neon). This liquid has a radiation length of 125 cm and an electron density of $9.28 \times 10^{22} \text{ cm}^{-3}$. A total of 44 400 γ 's with energy between 0.1 and 10 GeV were produced from a sample of about 20 000 π^+ -nucleon interactions. The γ flux was monitored from electron-positron pair production in the bubble chamber. The pairs were measured on precision measuring machines in order to determine the energy spectrum of the γ flux, which is shown in Fig. 5. The details of the γ -pair scanning, measurement, and detection efficiency calculations have been described in previous publications.¹⁶ The results of our studies show that, after all corrections, the γ -flux measurement from the e^+e^- pairs has a systematic uncertainty of less than 6%. This is

essentially independent of γ energy. The electron-momentum measurements were properly corrected for ionization and bremsstrahlung energy losses, and the γ energy, as determined from the sum of the electron-pair energies, was determined to about 8% (σ_E/E).

B. Scanning and measurement

The bubble-chamber photographs containing the 20 000 primary π^+ -nucleon interactions were doubly scanned for Compton electrons. Any single negative track that was minimum ionizing and pointed back to the production point within 10° was accepted as a Compton-electron candidate. All positive tracks satisfying the criteria applied to negative tracks were also accepted in scanning. Most of the positive tracks are from small-angle np and K^0p charge-exchange scattering and do not, in fact, represent a Compton-electron background. However, they were useful in putting upper limits on certain backgrounds that are nearly symmetric between positive and negative tracks (see the discussion below).

Fiducial-volume cuts were applied which ensured measurability of the e^- tracks near the edge of the bubble chamber. In addition, a minimum neutral flight path was imposed to avoid confusion with knock-on e^- from charged tracks near the interaction origin.

The events found in the two complete scans were merged, yielding a sample of data consisting of 408 Compton-electron candidates and 62 positive tracks deliberately included for background-monitor purposes. The scanning efficiency was studied as a function of momentum and found to have little variation. For the Compton electrons finally selected (see Sec. IIC) the scanning efficiency was

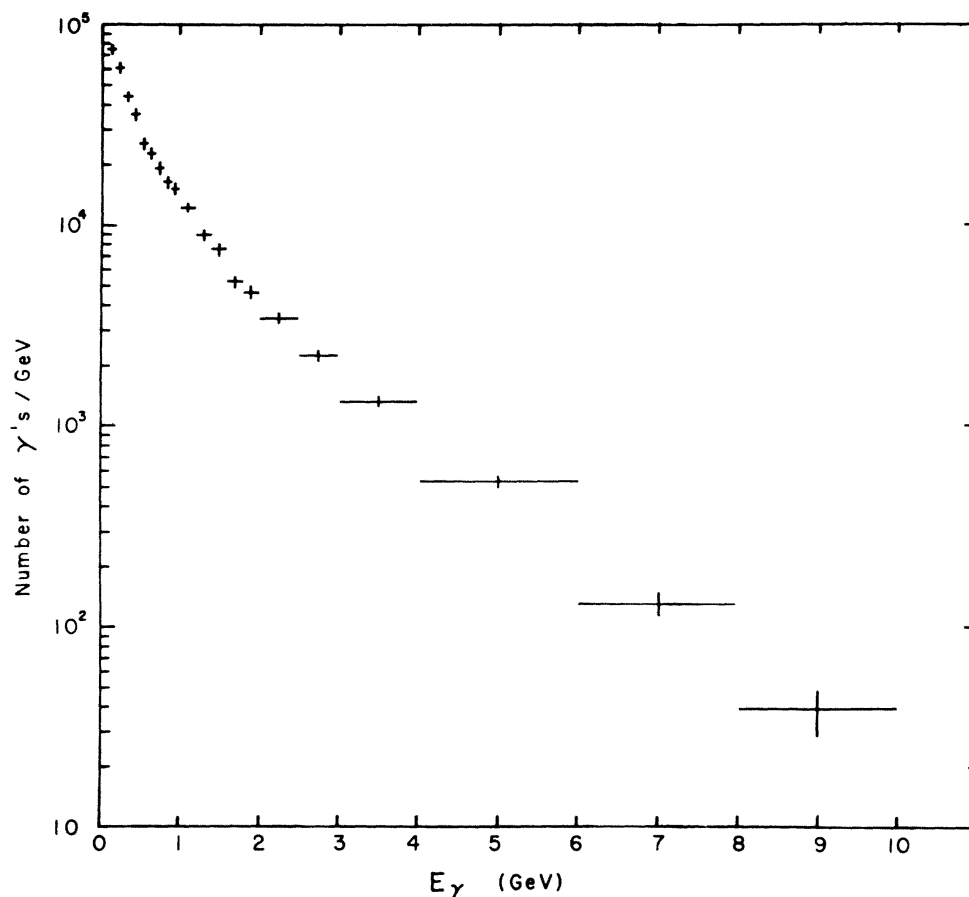


FIG. 5. Energy spectrum of the photons used in this experiment.

found to be $(95 \pm 2)\%$ for energies below 400 MeV and $(94 \pm 2)\%$ for energies above 400 MeV.

The momentum of each track was calculated from curvature measurements made directly on the scan table. This procedure allows careful treatment of the problems caused by hard bremsstrahlung of the electrons at little expense to measurement precision. The curvature measurements were converted to momenta and properly corrected for ionization and bremsstrahlung losses. The resulting average electron-momentum error is about 10% (σ_E/E).

C. Background corrections

There are three sources of background that must be removed from the Compton-electron candidates.

(i) *Unassociated Compton electrons.* We must reject those Compton electrons not coming from the primary hadronic interactions which were used to produce the primary photon flux (see Sec. II A). Unassociated Compton electrons may come from random hadronic interactions in the bubble-cham-

ber liquid or entrance window. In addition, e^+e^- pairs from photon conversions produce secondary bremsstrahlung photons that can in turn produce Compton electrons. These random, background Compton electrons were removed by making use of the measured angle between the neutral direction from the hadronic interaction to the electron origin and the direction of the electron itself. The angle was measured in projection on the scan table. Figure 6(a) shows the distribution of this angle for all Compton-electron candidates. The sharp peak near zero degrees is in marked contrast to the flat angular distribution found for positive tracks satisfying all the same scanning criteria [see Fig. 6(b)]. The solid curve in Fig. 6(a) shows our estimate of the contribution of unassociated Compton electrons to these data. The shape of this curve was obtained by taking the conversion vertex point and photon direction of measured e^+e^- pairs from one bubble-chamber photograph and adding these to the reconstructed primary vertex point of another, randomly selected, π^+ -nucleon interaction. The projected pointing angle of Compton electrons from these

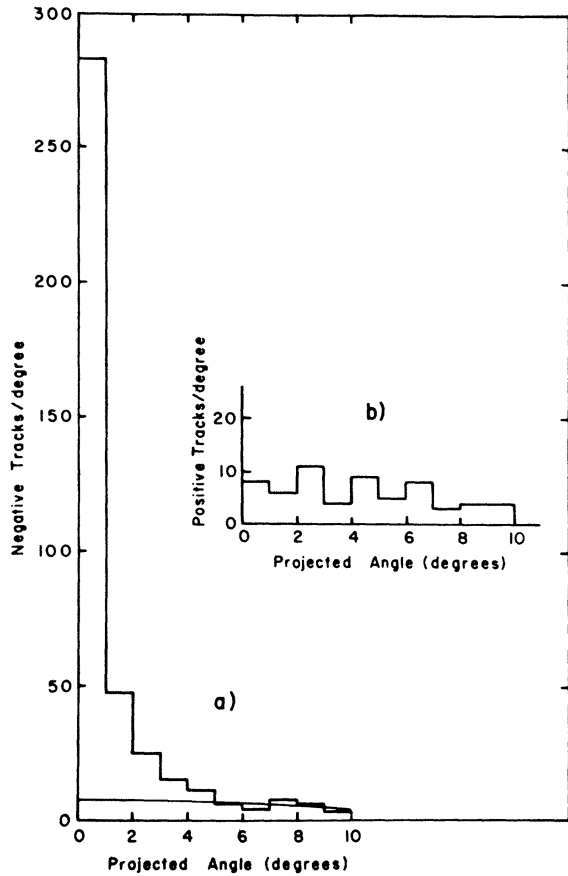


FIG. 6. (a) The distribution of the projected scattering angle of all Compton-electron candidates obtained in scanning. (b) The same distribution measured for positive tracks satisfying the Compton scan criteria.

randomly introduced photons was then calculated using a Monte Carlo program. The solid curve in Fig. 6(a) is the distribution of this angle, normalized to the observed Compton-electron candidates with pointing angles greater than 4° (taking into account a very small contribution expected for real Compton electrons). If we make a cut at 4° , then the background due to unassociated Compton electrons is 26 events out of 370, or about 7%. The 4° angle cut also removes some truly associated Compton electrons, but this is properly corrected for when we compare our data to QED theory (see Sec. IV).

(ii) *Asymmetric e^+e^- pairs.* A γ conversion into an e^+e^- pair with an undetected e^+ could fake a Compton electron. The e^+ would not be seen in the bubble chamber if either its range is very short or it annihilates in flight near the pair origin. We consider each of these effects separately and show that the combined background is no more than 2% of the accepted Compton-electron data.

Because of the relatively low density (0.265

g/cm^3) of our bubble-chamber liquid, we detect positrons down to a momentum of 1 MeV/c with high efficiency. Below this momentum the visibility gradually decreases in a manner that is difficult to measure quantitatively. We can, however, put an upper limit on the number of e^+e^- pairs with an unseen, short-range e^+ by making use of the symmetry with the number of e^+e^- pairs with an unseen e^- . Figure 6(b) shows no evidence for any peak in the pointing angle at zero degrees where an e^+e^- pair with unseen e^- would appear. Using this data, we can put an upper limit of three fake Compton electrons caused by e^+e^- pairs with unseen, short-range e^+ .

In addition to short-range e^+ , the e^+ can annihilate via $e^+e^- \rightarrow \gamma\gamma$ and fake Compton electrons. We have calculated this effect by taking each e^+e^- pair in our data and randomly repartitioning the e^+ and e^- energy sharing using standard QED theory. We then calculate the probability that the e^+ annihilates within 1 cm of the pair origin. A total of 5.4 events are predicted to fake Compton e^- via this process (a background of only 1.5%).

(iii) *Single negative hadrons.* The neutral hadrons coming from the primary π^+ -nucleon interaction can undergo decays or secondary interactions which produce apparent single negative tracks in the bubble-chamber liquid. All of these must have, of course, one or more short-range, unseen protons. We have considered the possibility that these might fake Compton electrons and find that the effect is negligible. The details of the argument are given below.

All neutron, Λ^0 and K^0 ($S = +1$), secondary interactions producing a negative particle involve at least three particles in the final state.¹⁷ These would result in a negative particle with a broad pointing angular distribution that would be removed by the same background subtraction that removed unassociated Compton electrons. The one interaction not falling into this category is $\bar{K}^0 n \rightarrow p K^-$ with both recoil proton and the nuclear-fragmentation protons unseen due to short range. For this particular interaction we have calculated the expected number of small angle K^- . The K_S^0 spectrum was obtained from measured $K_S^0 \rightarrow \pi^+ \pi^-$ decays and, together with known cross sections, used to calculate the number of \bar{K}^0 secondary interactions within our Compton-electron fiducial volume. We then scaled down the total number of expected $\bar{K}^0 n$ interactions by the ratio of the forward $\bar{K}^0 n \rightarrow K^- p$ cross section to the total cross section. The calculation is approximate, but the result shows that less than one background event comes from this process.

K^0 and Λ^0 decays cannot fake Compton electrons. A $K_S^0 \rightarrow \pi^+ \pi^-$ with short-range π^+ will always be

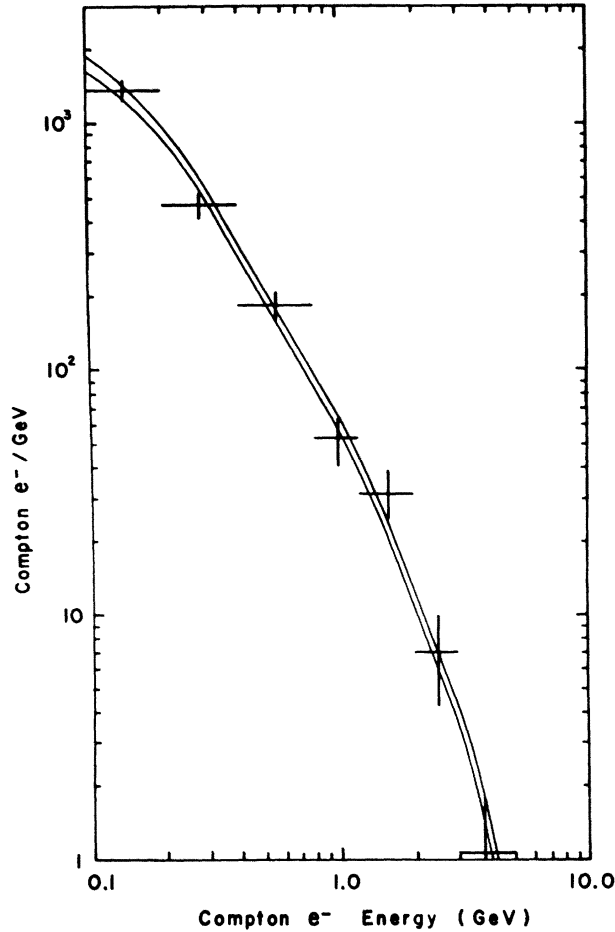


FIG. 7. A comparison of the measured Compton-electron spectrum (data points) to that predicted from QED theory. The two solid curves represent the uncertainty of the theoretical prediction which is based on measured e^+e^- pair production.

seen because of the subsequent $\pi^+ \rightarrow u^+ e^+$ decay. Λ^0 's with momentum greater than 250 MeV/c will always produce a decay proton that is seen. The number of Λ^0 's with momentum less than 250 MeV/c is small and the decays occur so close to the origin that our minimum neutral path length cut reduces this background to a negligible level.

III. THE COMPTON-ELECTRON DATA

The final sample of Compton electrons consists of 357 events which cover the energy range from 0.1 to about 5 GeV. The differential energy spectrum is plotted in Fig. 7 and tabulated in Table I. The table also presents a differential summary of all the background corrections that were discussed in Sec. II C. Because of the small backgrounds and high detection efficiency in this experiment, the systematic uncertainties in the Compton-electron energy spectrum are small compared to the statistical errors. The errors quoted contain our best estimate of all these effects.

As discussed in the next section, the data presented in Fig. 7 provides our best experimental test of QED theory. We can, in addition, measure production cross sections which depend on the energy spectrum of the photon flux in this experiment (see Fig. 5). The cross section for the production of Compton electrons with energy greater than 0.1 GeV by photons with energy greater than 0.1 GeV is 1.83 ± 0.11 mb. This number is systematically uncertain by 8% due to the photon-flux normalization and target-electron density. For orientation purposes we present in Fig. 8 the measured ratios of Compton electrons to photons and of e^+e^- pairs to photons in the energy range from 0.1 to 5.0 GeV.

TABLE I. The Compton-electron data showing all background corrections. The last column presents the fully corrected data.

Energy bin (GeV)	Observed events	Unassociated Compton electrons	Backgrounds			Single negative hadrons	Final Compton-electron events ^a
			e^+ annihilation from e^+e^- pairs	e^+ unseen from e^+e^- pairs			
0.1-0.2	141	9.5 ± 2.6	1.8 ± 0.9	0	0	136 ± 13	
0.2-0.4	101	11.1 ± 3.3	1.6 ± 0.8	0	0	93 ± 11	
0.4-0.8	73	3.6 ± 1.6	1.0 ± 0.5	0	0	73 ± 9	
0.8-1.2	21	0.8 ± 0.8	0.4 ± 0.2	0	0	21.1 ± 5.0	
1.2-2.0	25	0.9 ± 0.9	0.4 ± 0.4	0	0	25.3 ± 5.7	
2.0-3.0	7	0.3 ± 0.3	0.2 ± 0.2	0	0	7.0 ± 2.8	
3.0-5.0	2	0.0 ± 0.3	0.0 ± 0.1	0	0	2.1 ± 1.5	
Total	370	26.2 ± 4.7	5.4 ± 1.4	<3	<1	357 ± 22	

^aFully corrected for scanning efficiency.

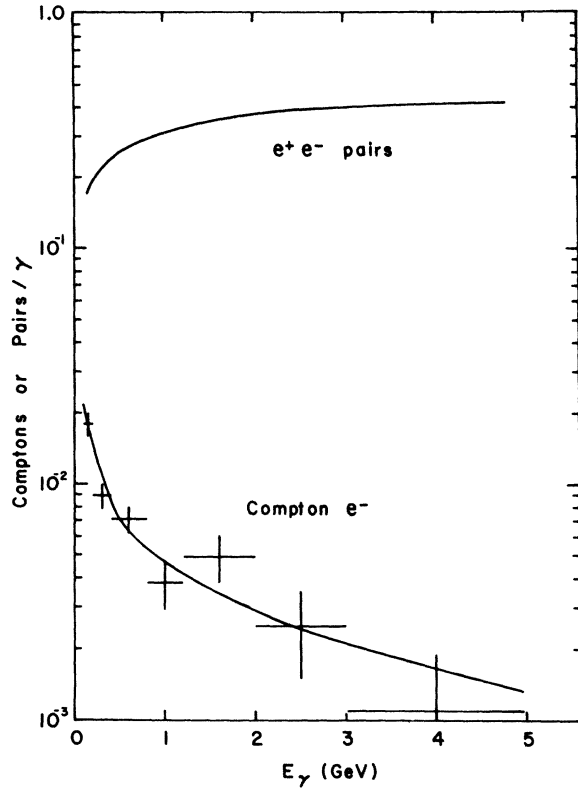


FIG. 8. The number of e^+e^- pairs produced per photon compared to the number of Compton electrons produced per photon. The solid curve through the data points is the prediction of QED theory.

IV. COMPTON-ELECTRON THEORY

As discussed in Sec. IA, the QED prediction for Compton scattering which includes higher-order corrections [see Figs. 2(a) and 2(b)] differs little from the cross section calculated using the lowest-order diagram alone [Fig. 1(a)].¹⁸ Therefore, for simplicity, we compare our data directly to the well-known Klein-Nishina formula which is accurate (see the solid curve in Fig. 4) to within our experimental errors. For an unpolarized photon of energy E , the differential-scattering cross section is given by

$$\frac{d\sigma}{dE'} = (\pi r_0^2) \left(\frac{m}{EE'} \right) \left[1 + \left(\frac{E'}{E} \right)^2 - \left(\frac{E'}{E} \right) \sin \theta \right], \quad (1)$$

where E' is the energy of a photon scattered at an angle θ [see Fig. 1(b)], m is the electron mass, and r_0 is the classical electron radius. In order to compare the predictions of this differential cross section to our data, we first calculate the cross section for the production of electrons with kinetic energy between T_1 and T_2 by a photon of energy E :

$$\sigma(E; T_1, T_2) = (\pi r_0^2) \left(\frac{m}{E} \right) \left\{ \ln \left(\frac{E - T_1}{E - T_2} \right) + \frac{1}{2E^2} [(E - T_1)^2 - (E - T_2)^2] \right\}, \quad (2)$$

where we have used $T = E - E'$ and have neglected terms in which $m/E \ll 1$. It then follows that for the photon spectrum used in our experiment, the number of Compton electrons expected in the energy range T_1 to T_2 is given by

$$N_c(T_1, T_2) = \sum_{i=1}^{N_p} \frac{\lambda_p(E_i)}{\lambda_c(E_i; T_1, T_2)}, \quad (3)$$

where $\lambda_p(E)$ is the e^+e^- pair production length for a photon of energy E ,¹⁹ and $\lambda_c(E; T_1, T_2) = [\sigma(E; T_1, T_2) \rho_e]^{-1}$ is the production length for a Compton electron in the energy range T_1 to T_2 by a photon of energy E . The sum is over the energy spectrum of the e^+e^- pairs (not the photon-energy spectrum). Since the photon-flux monitor in our experiment is e^+e^- pairs, then Eq. (3) gives us a very direct prediction of the expected number of Compton electrons. Systematic errors in the liquid density cancel out as do the effects of fiducial-volume cuts. The result is relatively insensitive to errors in the H_2 versus Ne fractional composition of our liquid.

Two experimental corrections must be made to the numbers of Compton electrons predicted by Eq. (3) before they can be compared to the data given in Table I. First, the detection efficiency for the sample of e^+e^- pairs used in the sum must be included. This is done by including an experimental weight w_i in the sum where w_i is the reciprocal of the e^+e^- pair detection efficiency over the fiducial volume in which the Compton electrons were collected. The average value of w_i is 1.32. Finally, we must take into account the 4° projected angle cut applied in selecting the Compton-electron data. The procedure is as follows. The kinetic energy of an electron emitted at an angle θ_e from a photon of energy E is given by:

$$T_e(E, \theta_e) = \frac{2mX}{(1-X)}, \quad (4)$$

where

$$X = \left(\frac{E \cos \theta_e}{E + m} \right)^2.$$

For a given azimuthal angle ϕ_e , all Compton electrons are lost from our data sample if their energy is less than T_{\min} , where

$$T_{\min} = T_e [E, \tan^{-1}(\tan 4^\circ / \sin \phi_e)]. \quad (5)$$

This cut can be easily incorporated into the pre-

TABLE II. The number of Compton electrons predicted from QED theory. The last column compares this prediction to the observed number of events.

Energy bin (GeV)	Predicted Compton-electron events	$\frac{\text{Predicted events}}{\text{Observed events}} = R$
0.1-0.2	135 \pm 8	0.99 \pm 0.11
0.2-0.4	117 \pm 6	1.26 \pm 0.17
0.4-0.8	63 \pm 3	0.87 \pm 0.12
0.8-1.2	25.2 \pm 1.2	1.2 \pm 0.3
1.2-2.0	17.5 \pm 0.8	0.7 \pm 0.2
2.0-3.0	6.7 \pm 0.4	1.0 \pm 0.4
3.0-5.0	3.3 \pm 0.2	1.6 \pm 1.1
Total	368 \pm 10	1.03 \pm 0.07

dictions made by Eq. (3) if we average over the angle ϕ_e for each e^+e^- pair in the sum.

The resulting theoretical prediction is bounded by the solid curves shown in Fig. 7. The number of Compton electrons predicted in each energy bin is tabulated in Table II. The errors quoted arise from estimated uncertainties in the e^+e^- pair detection efficiency w , and the calculated pair-production length $\lambda_p(E)$.

V. COMPARISON OF THEORY TO EXPERIMENT

The total number of measured Compton electrons, 357 ± 22 , agrees well with the theoretical

prediction of 368 ± 10 . Figure 7 shows that the differential energy spectrum also agrees with theory. A more quantitative evaluation of this is presented in Table II where the last column shows the ratio R of the predicted to observed numbers of Compton electrons in various energy ranges. For Compton electrons with energies between 0.1 and 5.0 GeV, the value of R is 1.03 ± 0.07 ; for energies between 0.8 and 5.0 GeV, R is 0.95 ± 0.14 .

To the best of our knowledge, this is the first experimental measurement of Compton-electron production rates at energies above 1 GeV. In addition, it is the first published measurement in which the photon source is from the decay of a hadron. This experiment finds no deviation from QED predictions in this new physical domain.

ACKNOWLEDGMENTS

We thank Professor Lawrence E. Evans for very useful discussions of the theory of Compton scattering. It is a pleasure to acknowledge the diligent work done in this experiment by our scanning staff. We also thank the personnel at SLAC for their valuable assistance during the data-taking run in the 82-in. bubble chamber.

This work was supported by the Department of Energy, Contract No. E-(40-1)-3065.

¹A. H. Compton, Bull. Nat. Res. Council. (U.S.) No. 20, 19 (1922); Phys. Rev. **21**, 207 (1923); **21**, 483 (1923).

²O. Klein and Y. Nishina, Z. Phys. **52**, 853 (1929).

³I. Tamm, Z. Phys. **62**, 545 (1930).

⁴I. M. Brown and R. P. Feynman, Phys. Rev. **85**, 231 (1952).

⁵Till B. Anders, Nucl. Phys. **87**, 721 (1967).

⁶K. J. Mork, Phys. Rev. A **4**, 917 (1971); there is a misprint in Eq. 6.2 of this paper. The coefficient of the $\ln|k|$ term should be $-\frac{5}{6}\pi^2$ instead of $-\frac{5}{6}$ (private communication from K. J. Mork).

⁷This radiative correction contains an infrared divergence that is cancelled by a similar term that arises in the double-scattering cross section. Since only the sum has physical significance, this causes no problem, and we have ignored these divergent terms in presenting the cross sections given in Fig. 4. See Ref. 4 for a further discussion of this point.

⁸F. Mandl and T. H. R. Skyrme, Proc. R. Soc. London **A215**, 497 (1952).

⁹Michael Ram and P. Y. Wang, Phys. Rev. Lett. **26**, 476 (1971); **26**, 1210(E) (1971).

¹⁰In doing this calculation we used Eqs. (6.5) and (6.6) in Ref. 6 and the numerical-integration results given in the last column of Table IV.

¹⁶We caution the reader that this final estimate of the net correction to the Klein-Nishina total cross section has an uncertainty of a few percent due to the limitations of the numeric integration results presented in Ref. 6. This is not important for the purpose of our

present work where our experimental errors are 7%.

¹²F. H. Coensgen, University of California Radiation Laboratory Report UCRL-2413, 1953 (unpublished).

¹³L. V. Kurnosova *et al.*, Zh. Eksp. Teor. Fiz. **30**, 690 (1956) [Sov. Phys.—JETP **3**, 546 (1956).]

¹⁴John D. Anderson *et al.*, Phys. Rev. **102**, 1626 (1956).

¹⁵B. Gittelman *et al.*, Phys. Rev. **171**, 1388 (1968).

¹⁶J. R. Elliott *et al.*, Phys. Rev. D **15**, 1851 (1977);

J. R. Elliott *et al.*, Phys. Rev. D **17**, 83 (1978).

¹⁷The two-body Λ^0 reaction $\Lambda^0 n \rightarrow \Sigma^- p$ would be rejected from our data sample during scanning.

¹⁸This is true not only for the total cross section but also for the differential electron spectrum in the scattering-angle range measured in our experiment. For a detailed discussion of this point see Ref. 5, where the effect of radiative corrections and double Compton scattering on the scattered-electron spectrum is studied.

¹⁹Pair production cross sections have been measured to accuracies of on the order of 1 or 2% and found to agree with QED calculations. See, for example, E. Malamud, Phys. Rev. **115**, 687 (1959) for an experimental measurement using 1 GeV photons. For theoretical calculations, see J. W. Motz *et al.*, Rev. Mod. Phys. **41**, 581 (1969) and T. M. Knafl, Nucl. Instrum. Methods **83**, 217 (1970). For the purpose of error estimates in this paper we have included uncertainties in the calculated pair-production cross section of 3% for photons below 0.4 GeV and 2% above 0.4 GeV.

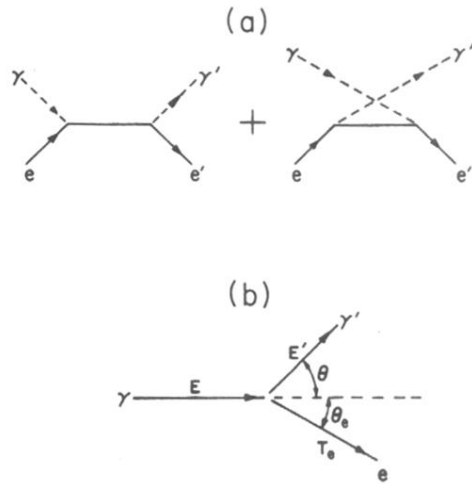


FIG. 1. (a) The lowest-order Feynman diagrams for Compton scattering. A QED calculation using these diagrams results in the Klein-Nishina formula. (b) Definition of the laboratory scattering variables used throughout this paper.

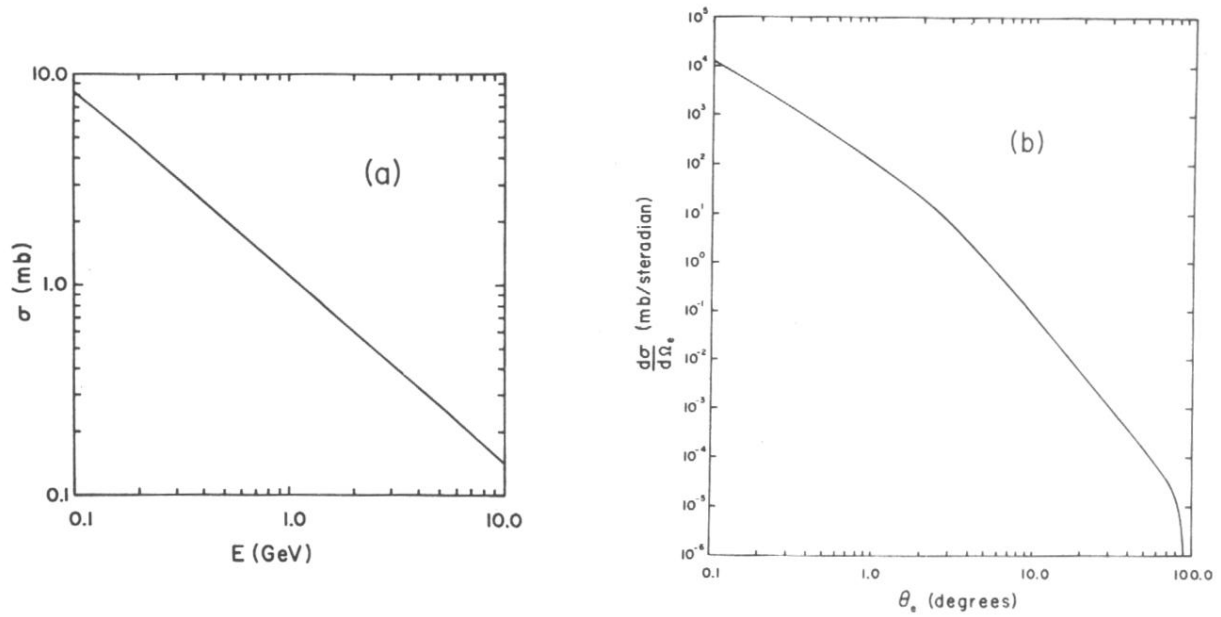


FIG. 2. Cross sections calculated using the Klein-Nishina formula; (a) the total cross section as a function of photon laboratory energy and (b) the laboratory differential cross section in terms of the scattered electron angle.

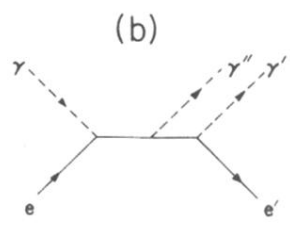
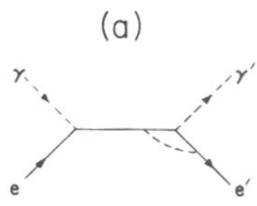


FIG. 3. (a) A typical radiative correction to single Compton scattering. (b) A Feynman diagram representing double Compton scattering.

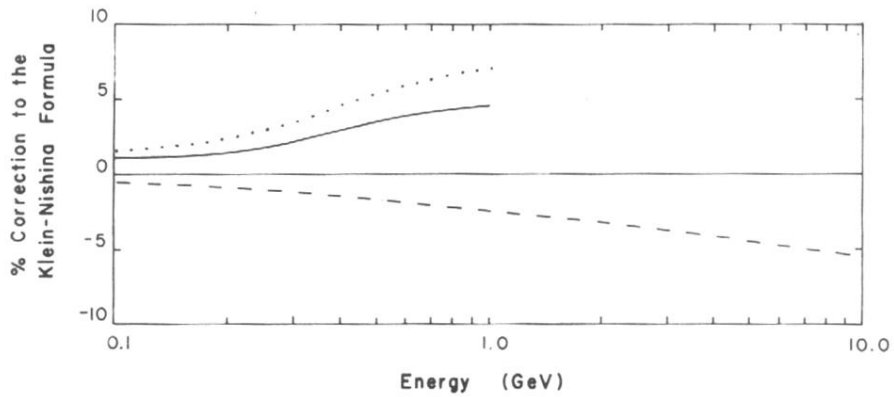


FIG. 4. The dashed curve shows the percentage correction to the Klein-Nishina formula caused by radiative corrections of the type shown in Fig. 3(a). The dotted curve shows the double-scattering cross section expressed as a percentage of the Klein-Nishina formula. The total percentage correction to the Klein-Nishina formula due to both effects is given by the solid curve.

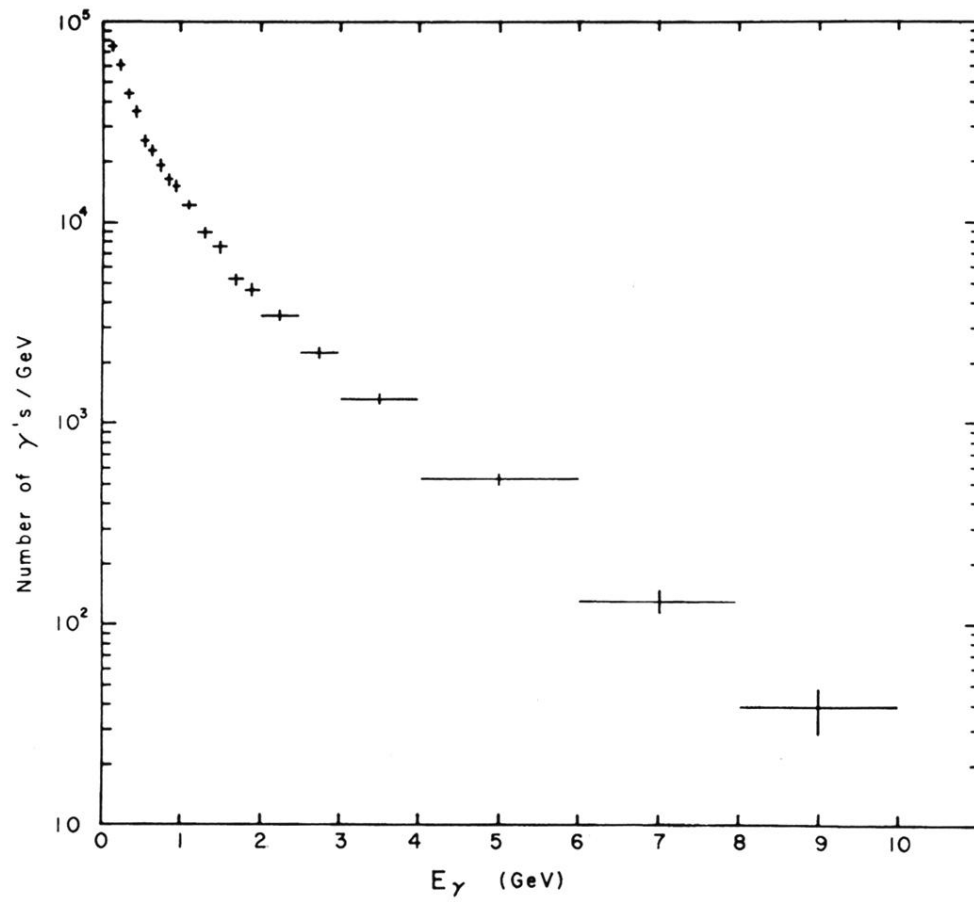


FIG. 5. Energy spectrum of the photons used in this experiment.

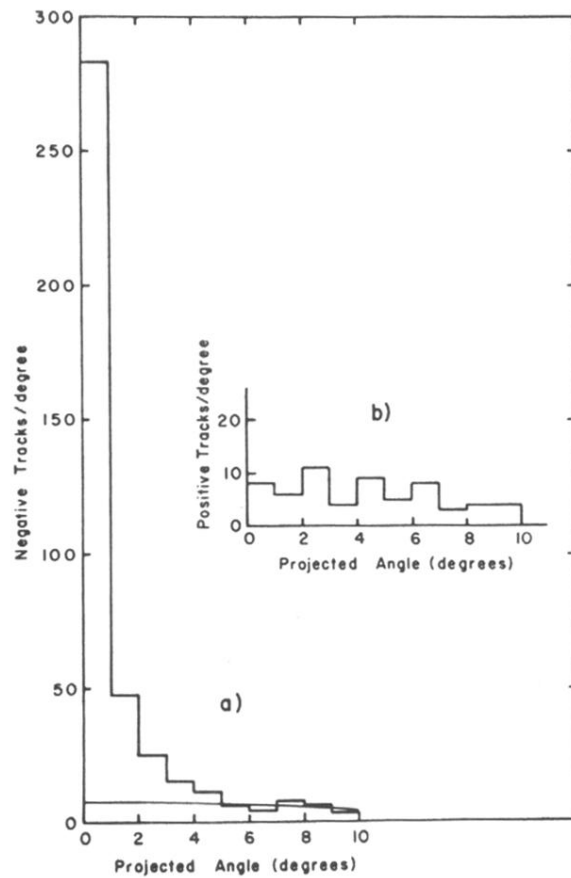


FIG. 6. (a) The distribution of the projected scattering angle of all Compton-electron candidates obtained in scanning. (b) The same distribution measured for positive tracks satisfying the Compton scan criteria.

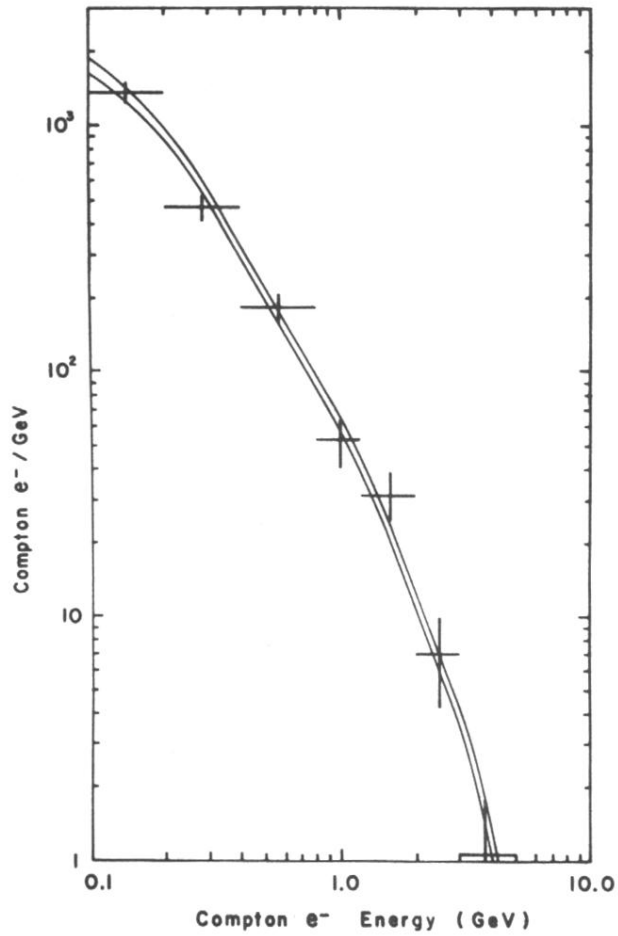


FIG. 7. A comparison of the measured Compton-electron spectrum (data points) to that predicted from QED theory. The two solid curves represent the uncertainty of the theoretical prediction which is based on measured e^+e^- pair production.

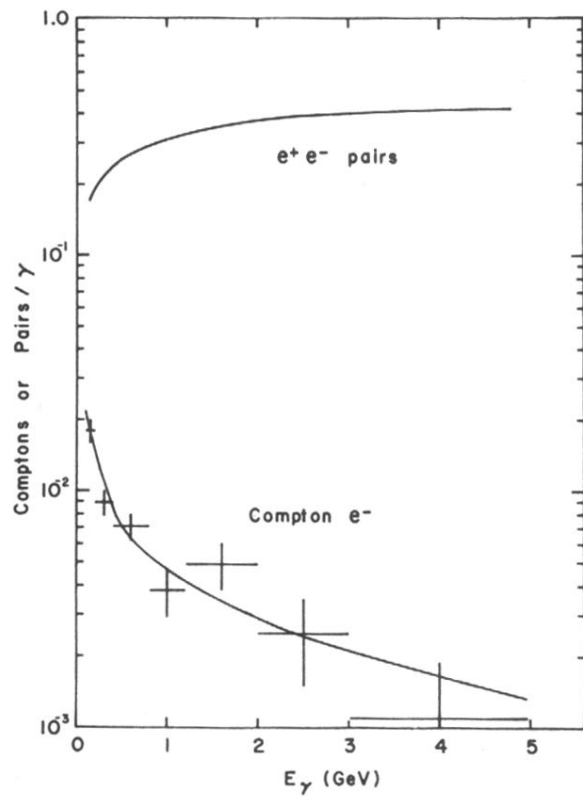


FIG. 8. The number of e^+e^- pairs produced per photon compared to the number of Compton electrons produced per photon. The solid curve through the data points is the prediction of QED theory.